Fluctuations of Broadband Acoustic Signals in Shallow Water

Mohsen Badiey
College of Earth, Ocean, and Environment
University of Delaware
Newark, DE 19716
Phone: (302) 831-3687   Fax: (302) 831-3302   Email: badiey@udel.edu

LONG-TERM GOALS

The long-term goal of this project is to obtain quantitative understanding of the physical mechanisms governing broadband (50 Hz to 50 kHz) acoustic propagation, reflection, refraction, and scattering in shallow water and coastal regions in the presence of temporal and spatial ocean variability.

OBJECTIVES

The scientific objective of this research is to understand acoustic wave propagation in a dynamic environment in two frequency bands: Low (50 Hz to 500 Hz) and Mid-to-High (500 Hz to 50 kHz). The goal for the low frequency band is to assess the effects of internal waves on acoustic wave propagation, with an emphasis on the mechanisms that cause significant temporal and spatial acoustic intensity fluctuations. The goal for the mid-to-high frequency band is to assess the effects of water column and dynamic sea surface variability, as well as source/receiver motion on acoustic wave propagation for underwater acoustic communications, tomography, and other applications.

APPROACH

The project combines theoretical, experimental, and modeling efforts to improve our understanding of broadband acoustic wave propagation in a dynamic shallow water environment. Studies in the low frequency band have been focused on the data from the SW06 experiment for both stationary [1] and moving sources with vertical and horizontal array receivers. A 3D acoustic propagation model has been utilized and a detailed 3D environment data required as input to the model has been constructed using temperature and radar image data. Improvement has been made with better estimation of the internal wave front curvature and better estimation of the receiver positions.

Studies in the mid-to-high frequency band have utilized data collected at KAM08 [2] and KAM11 [3] experiments. The effects of sea surface, including surface bubbles, and water column variability on acoustic wave propagation have been investigated using Parabolic Equation (PE) model. A time evolving nonlinear sea surface wave model is being developed to realistically simulate the sea surface and wave breaking to determine the location of surface bubbles generation. To take into account the out-of-plane acoustic scattering and the directionality of the surface wave, the PE acoustic propagation model is being extended to 3D.

1. REPORT DATE **30 SEP 2014**	2. REPORT TYPE		3. DATES COVERED **00-00-2014 to 00-00-2014**
4. TITLE AND SUBTITLE **Fluctuations of Broadband Acoustic Signals in Shallow Water**			5a. CONTRACT NUMBER
			5b. GRANT NUMBER
			5c. PROGRAM ELEMENT NUMBER
6. AUTHOR(S)			5d. PROJECT NUMBER
			5e. TASK NUMBER
			5f. WORK UNIT NUMBER
7. PERFORMING ORGANIZATION NAME(S) AND ADDRESS(ES) **University of Delaware,College of Earth, Ocean, and Environment,Newark,DE,19716**			8. PERFORMING ORGANIZATION REPORT NUMBER
9. SPONSORING/MONITORING AGENCY NAME(S) AND ADDRESS(ES)			10. SPONSOR/MONITOR'S ACRONYM(S)
			11. SPONSOR/MONITOR'S REPORT NUMBER(S)
12. DISTRIBUTION/AVAILABILITY STATEMENT **Approved for public release; distribution unlimited**			
13. SUPPLEMENTARY NOTES			
14. ABSTRACT			
15. SUBJECT TERMS			

16. SECURITY CLASSIFICATION OF:			17. LIMITATION OF ABSTRACT	18. NUMBER OF PAGES	19a. NAME OF RESPONSIBLE PERSON
a. REPORT **unclassified**	b. ABSTRACT **unclassified**	c. THIS PAGE **unclassified**	**Same as Report (SAR)**	**16**	

WORK COMPLETED

1) Low Frequency Acoustic Wave Propagation
    A 3D PE model and a detailed 3D environment, reconstructed based on shipboard radar images and temperature data [4], are developed to study both stationary and moving sources propagation scenario with vertical and horizontal array receivers in the presence of internal waves. The model-data agreement was considerably improved when the curvature of the internal wave fronts was included in the model compared to straight wave front assumption. The model was further improved by utilizing better estimation of the internal wave curvature and receiver locations. It is shown that the model not only can reproduce the mechanisms (focusing-defocusing, interference, etc.) of the acoustic intensity fluctuation, but is also able to quantitatively predict the time and location of specific details given a high quality reconstruction of 3D environment as parameter.

2) Mid-to-High Frequency Acoustic Wave Propagation
    We have continued our analyses of data from KAM08 and KAM11 to assess the effects of the environment on the acoustic wave propagation. For modeling, time-evolving rough sea surfaces used as boundaries in the PE model were re-generated using waverider buoy data from KAM08 and KAM11. A rough surface model was used from our previous results [5] and developed and included in the BELLHOP Ray model to study the effects of surface roughness on acoustic propagation. Results from surface wave acoustic stiration patterns in form of arrival times from the Ray model compared well with data and specific features relevant to the acoustic communication research are being studied in detail.

RESULTS

A.   Low Frequency Acoustic Wave Propagation in the Presence of Shallow Water Internal Waves

During SW06, detailed measurements of the time-varying ocean environment were made while simultaneously acoustic signals were transmitted between various source and receiver pairs. The time-varying environment induced by internal waves was recorded by an array of moored thermistor chains, as well as by the attending research vessels. Using a mapping technique described in a journal paper [4] the 3D temperature field for over a month of internal wave events was reconstructed. The results of this mapping are used for the statistical analysis of the internal wave parameters, such as the wave propagation speed, direction, amplitude, etc. The reconstructed environment results can be utilized to study the internal wave impact on 3D acoustic propagation in waveguides. Here we present the environmental data as well as acoustic data during one of the IW events to show the time-evolving modal features of the broadband acoustic propagation. We note here that the frequency band that we show covers 87.5 to 330 Hz. Details of these results are shown in our presentations during the 166th Acoustical Society meeting in San Francisco [6, 7].

1. Temporal coherence of normal modes during SW06

During the Shallow Water Acoustic Experiment 2006 (SW06) conducted on the New Jersey continental shelf, the three-dimensional (3D) temperature field for one month of internal wave (IW) events has been reconstructed. The aforementioned IW events, with the angle between the acoustic track and the IW front varying from -8° to 83°, were measured while simultaneously acoustic signals were transmitted from fixed sources at an along-shelf distance of about 20 km with frequencies at 87.5-112.5Hz (m-sequence), 175-225Hz (m-sequence), and 270-330Hz (chirp) respectively. The acoustic signals were recorded by an L-shaped hydrophone array moored inside the area with IW measurements. Here, we analyze the acoustic data transmitted from fixed acoustic source with center frequencies at 100Hz, 200Hz and 300Hz respectively. The coherence of acoustic normal modes decomposed from the measured acoustic field accompany with the simultaneously measured IW events is obtained as a function of frequency and IW parameters. Regarding the events with small α (angle between the acoustic track and the IW front), four conclusions can be made: (1) selected modes start to de-correlate when the IW is approaching the acoustic source-receiver track; (2) the modes are de-correlated faster when the IW cover the acoustic source-receiver track, (3) the background IW or the tail of the IW shows effect on selected modes; (4) modes start to re-correlate after the IW fronts pass the acoustic source-receiver track.
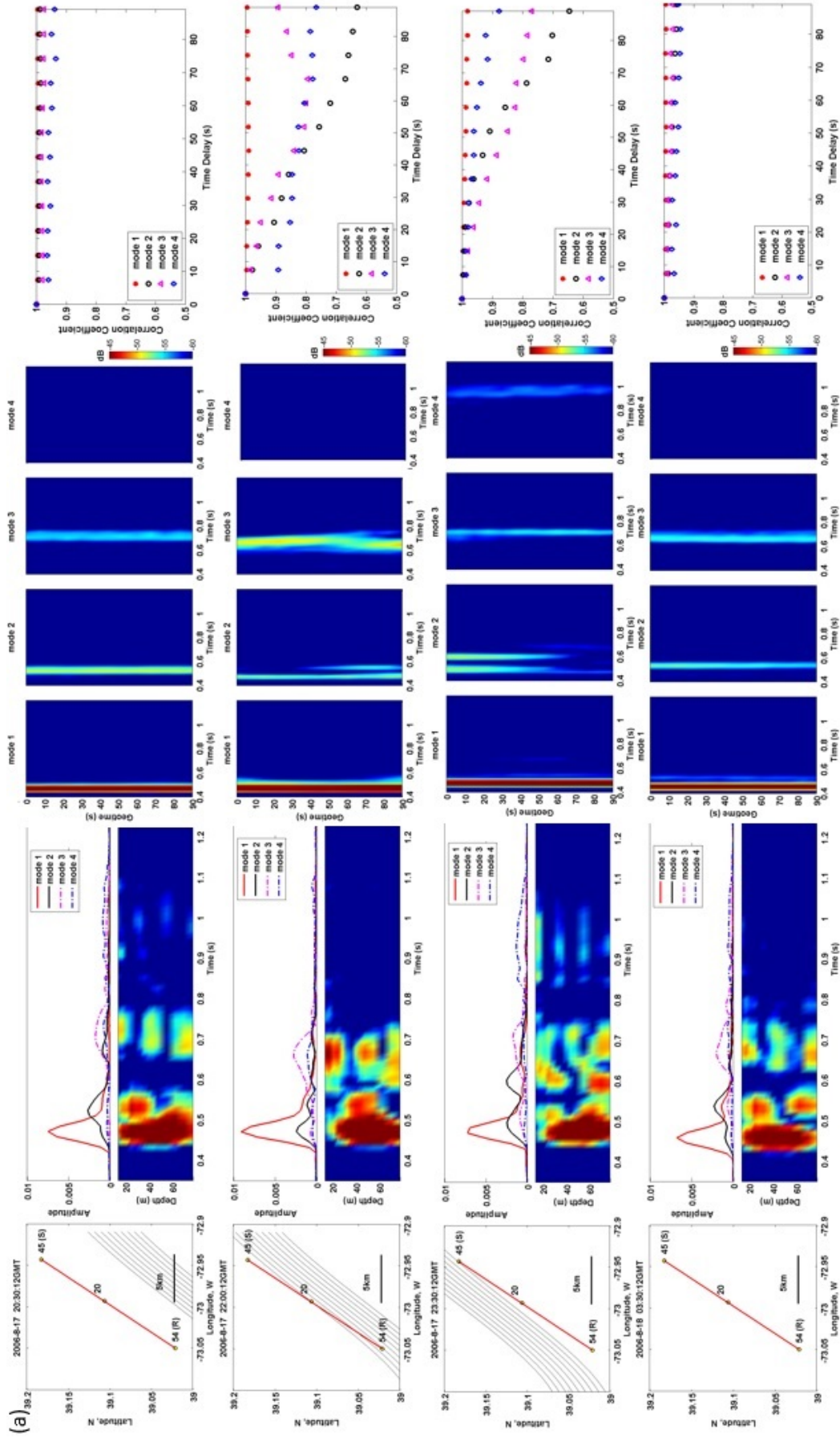
Fig. 1. (a) The picture collage is the example showing the evolution of IW event 50 (first column), vertical structure of received MSM100 signals (second column), decomposed modes as a function of geotime (third-six columns), and temporal coherence of normal modes at 100Hz (last column).
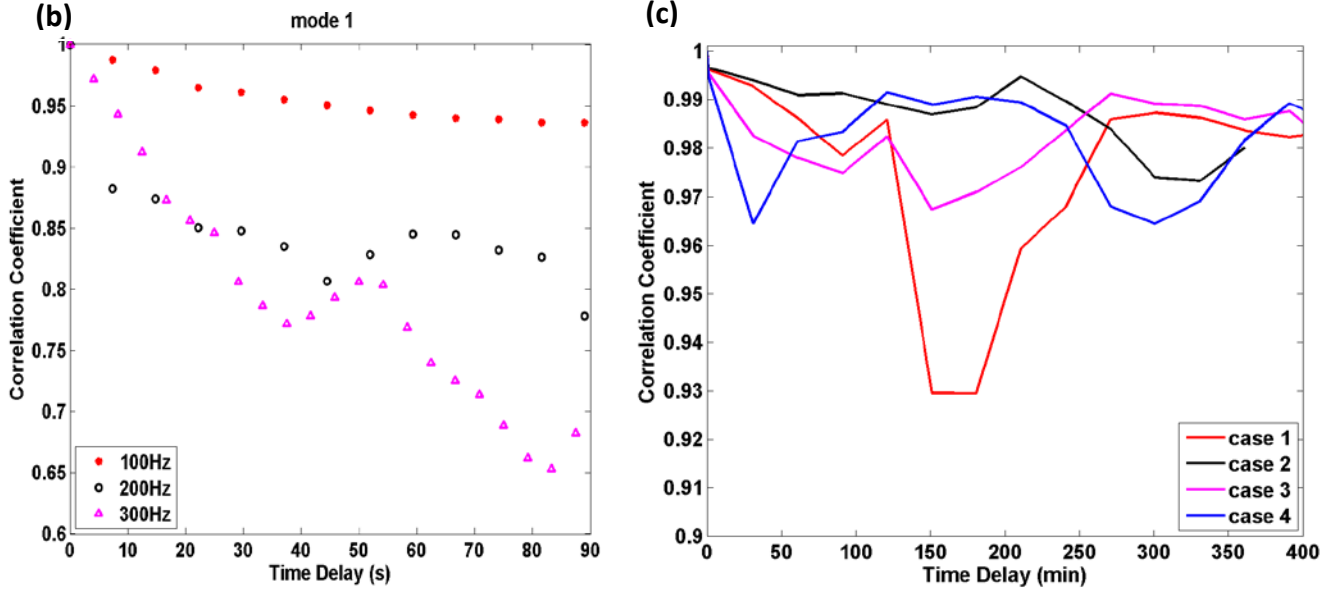
Fig. 1 (b) shows the short-time-lag correlation coefficient of mode 1 as a function of time delay at three different frequencies. The correlation coefficient is obtained by averaging the four 90-sec MSM100 transmissions results when IW fronts cover the acoustic source-receiver track. Fig.1 (c) shows the averaged long-time-lag correlation coefficient of mode 1 at 100Hz as a function of time delay for 4 different IW events. The received signal before the IW event is used as the reference (time delay is zero.). The first mode in all the four cases shows the re-correlation effect.

2. Low frequency acoustic normal modal communication in shallow water

We use model analysis to predict the performance of the time reversal processor. Equivalent to the matched-filtering operation, the time reversal processing outcome can be represented in terms of modes in the frequency domain [8, 9]:

$$Q(\omega) = \frac{2\pi}{r} \sum_m \frac{\exp(2img(\kappa_m)r)|\Psi_m(z_s)|^2}{|\kappa_m|}$$

where r is the source-receiver range, z_s is the source depth, and $\Psi_m(z)$ and κ_m are the mode shape and horizontal wavenumber associated with the m–th mode. Maximum length communication sequences (m-sequences) were transmitted during the SW06 experiment at multiple frequency bands. Here we analyzed the modal contributions to $Q(\omega)$ at 200 Hz during an internal wave event (Event 50). Significant acoustic fluctuations can be observed, as shown in the impulse responses over the receiver depth, when the internal wave packets affected the acoustic transmission. Such impact can also be observed in $Q(\omega)$. We use mode filtering techniques to decompose $Q(\omega)$ into individual mode's contributions [10]. At the 200 Hz central frequency, we observe that the first mode had the large contribution with or without the presence of the internal waves. During the internal wave presence, the contribution from the first mode experienced increased fluctuations.
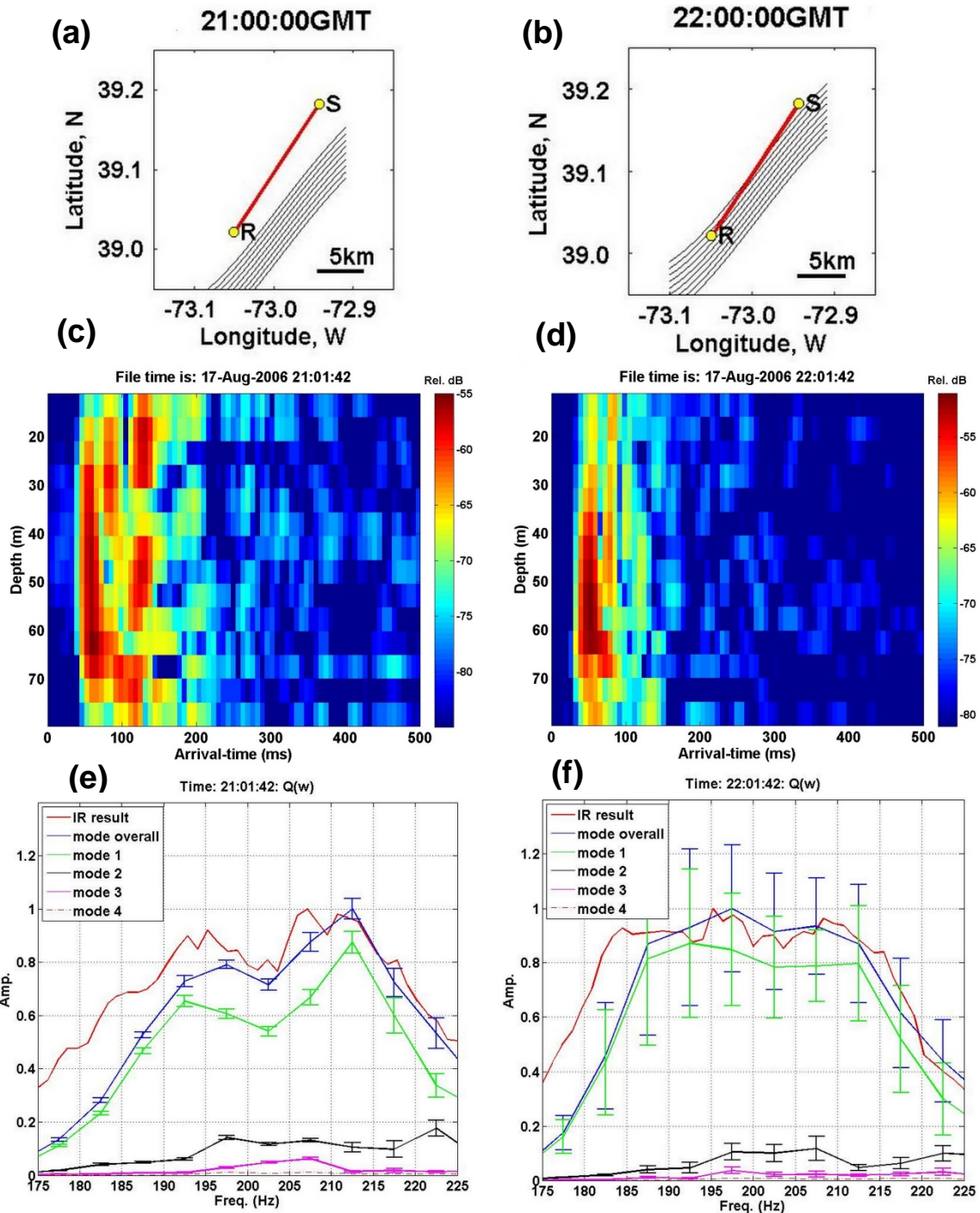
5

***Figure 2. Modal prediction of time reversal processing outcome, Q(w). Subplots (a), (c), and (e) show the relative
position between the acoustic track and the internal wavefronts, acoustic impulse responses (IR) at the receiver array,
and spectrum of Q(w), respectively, for 21:01 on Aug 17, 2006, when the internal waves did not intersect with the
acoustic track. Subplots (b), (d), and (f) show the processing results at an hour later, 22:01, when the internal waves
intersected with the acoustic track. Clear differences can be observed in the impulse response plots (c) and (d). For
example, the 3rd acoustic mode was strong at 21:01 in (c) while its strength was reduced significantly in (d). The
changes in impulse responses led to changes in Q(w), red curves in (e) and (f), which was predicted by a modal method
in good agreements. The first mode had the largest contribution to the overall Q(w) in both geotimes. However, when the
internal waves intersected with the acoustic track at 22:01 (subplot (f)), larger standard deviation of the first mode's
contribution was shown.***

6

3. Statistics of internal wave measurements during SW06 experiment

We have developed a statistical database from 30 recorded NLIW events during the SW06 experiment. These statistical data were obtained when the NLIW packet was located inside the thermistor farm such that the first front was close to the far edge of the farm. There are eight directly measured parameters and six derived ones. To the extent possible, we have followed Apel's notation in choosing these parameters. The mean value of each parameter, its standard deviation, and its estimated measurement error are listed in Table 1. The histograms of twelve parameters of the above set are shown in Fig. 3.

H_1 is the depth of the warm surface layer using the contour of the temperature at the middle of the thermocline as the reference. The value of H_2, which is the depth of the cold layer, is calculated from the difference between H_1 and the water depth at the thermistor farm (about 80 m). The soliton wavelength (λ_0) here is the horizontal width between the troughs of the first two solitons. The histograms of the first two soliton amplitudes (η_1 and η_2) are shown in Figs. 3(f) and 3(g), respectively. For 61% of the events, the value of $\eta_1 > \eta_2$, and the amplitude decay constant is $\beta = \frac{\ln(\eta_2/\eta_1)}{-\lambda_0} = 0.36 \text{km}^{-1}$. The half-amplitude width, Ls, is a characteristic scale of soliton that can be used to define the profile of these nonlinear waves. The number of solitons in a packet, n, is shown in Fig. 3(j). The NLIW propagation direction (α) is the direction measured within the thermistor farm with respect to true North. The average direction of the first group that contains 90% of the NLIW events is (309.5º) nearly perpendicular to the shelf-bottom isobath contours. For the second group, containing only 10% of the event, this direction is 13.4º, which is nearly parallel to the isobath contours. These waves are likely radiating from the Hudson Canyon, rather than from the shelfbreak. Assuming the NLIW speed within the thermistor farm is constant, we obtained that the propagation speed is 0.8 *m/s* falling into the range of its typical scale shown in Table 1. We next look at the slope of NLIW faces (designated as K here). In this report, we define $K = Ls/\eta_1 = 36.4$. Its histogram is shown in Fig.3 (i). Using the measured NLIW propagation speed (v), the packet length (L) and spacing between packets (D) can be estimated by estimated by $L(i) = [T_n(i) - T_1(i)] \times v(i)$ and $D(i) = [T_1(i+1) - T_1(i)] \times v(i)$, where $T_1(i)$ and $T_n(i)$ are the times when the first and last soliton of the ith NLIW packet arrive at the thermistor farm, respectively. The calculated results are shown in Figs. 3 (k) and (l). The NLIW front curvature is another parameter of great importance calculating 3D acoustic propagation. In this paper, we only recognized 4 NLIW events exhibiting obvious curved fronts within the thermistor farm area. Other events with the radius larger than 10 km exhibit almost straight NLIW fronts in this 4 km by 4 km area. The average value of R_c in the 4 events is 4.2 km.

In describing the aforementioned statistics, we consider the accuracy of the measurements, i.e. the error in measuring these values. One source of measurement error is likely due to the array element spatial and temporal resolutions and their spatial movement during the experiment (i.e. mooring motion). The accuracy of a particular parameter value would depend on the spatial position (in 3D) of the array farm in geotime. All the measurements during the passage of the NLIW are made using the same spatial and temporal variations. The uncertainties of the eleven parameters coming from the array elements vertical resolution (2.1 m), temporal resolution (15 sec) and their spatial movement (1.2 m in vertical and 5.0 m in horizontal plane) are obtained. The uncertainty of the number of solitons in a packet is comparable to the square root of the number according to Poison statistics. All the calculated uncertainties are listed in the last column of Table 1.
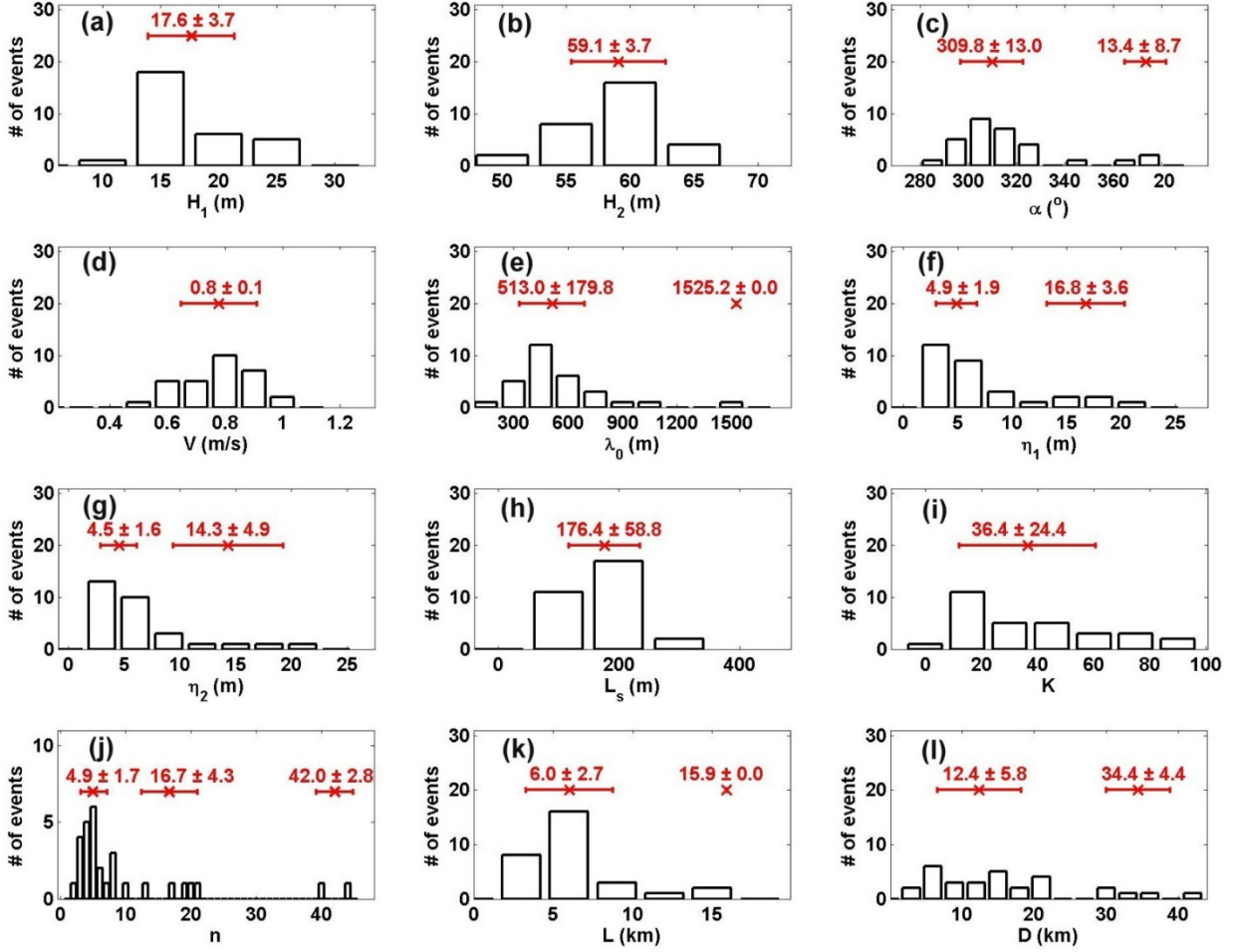
Figure 3 Histograms of (a) Upper layer depth; (b) Lower layer depth; (c) Propagation direction with respect to true North; (d) Propagation speed; (e) Wavelength; (f) 1st solition amplitude; (g) 2nd solition amplitude; (h) Soliton width; (i) Slope of NLIW faces; (j) Number of solitons in a packet; (k) Packet length; (l) Packet spacing.

Table 1. NLIW characteristic parameters

Characteristic(Symbol)	Unit	Typical Scale	SW06 Results	Uncertainty
Upper Layer Depth(H_1)	m	$5-25$	17.6 ± 3.7	2.4
Lower Layer Depth(H_2)	m	$30-200$	59.1 ± 3.7	2.4
Wavelength(λ_0)	m	$100-1000$	$513.0 \pm 179.8^{\square}$	5.0
1st Amplitude(η_1)	m	$0-30$	$4.9 \pm 1.9^{\square}, 16.8 \pm 3.6^{\triangle}$	2.4
2nd Amplitude(η_2)	m	$0-30$	$4.5 \pm 1.6^{\square}, 14.3 \pm 4.9^{\triangle}$	2.4
Solition Width(L_s)	m	100	176.4 ± 58.8	5.0
Number of Solitons(n)	$d.u.$	$1-20$	$4.9 \pm 1.7^{\square}$	2.2
			$16.7 \pm 4.3^{\triangle}$	4.1
			$42.0 \pm 2.8^{\diamond}$	6.5
Direction(α)	$deg.(^{\circ})$	a.s.	$309.5 \pm 13.0^{\square}, 13.4 \pm 8.7^{\triangle}$	0.2
Speed(V)	m/s	$0.5-1.0$	0.8 ± 0.1	0.003
Slope of IW faces(K)	$d.u.$	$5-100$	36.4 ± 24.4	19.0
Packet Length(L)	km	$1-10$	$6.0 \pm 2.7^{\square}, 15.9^{\triangle}$	0.02, 0.06
Packet Spacing(D)	km	$15-40$	$12.4 \pm 5.8^{\square}, 34.4 \pm 4.4^{\triangle}$	0.04, 0.11
Decay constant(β)	km^{-1}	$0.1-1.0$	$0.36 \pm 0.33^{\star}$	$\star$
Radius of curvature(R_c)	km	$15-\infty$	$4.2^{\star}$	$\star$
Coherence length(L_{coh})	λ	$20-40$	$28.9 \pm 24.9^{\star}$	8.1

d.u. : dimensionless unit; a.s. : across shelf; λ : acoustic wavelength; $\star$: explaination in text; $\square$: Group1; $\triangle$: Group2; $\diamond$: Group3

4. Acoustic modeling using statistics of internal waves

In order to model low-frequency acoustic wave propagation in a 3D waveguide with aforementioned internal waves, the NLIW fields are generated using the NLIW straight line front assumption and the extracted parameters following the Apel's NLIW notation. Ten of the thirty generated NLIW fields show small angles (±10º) between the NLIW front and acoustic track. Using the ten NLIW fields as input to a 3D Parabolic Equation model, we simulate the acoustic intensity of a 300 Hz signal similar to one of the source signals at 20 km range during SW06 experiment. Figure 4 (a) shows the reconstructed temperature field at 20m water depth using parameters extracted from event #72 in SW06 experiment, Aug. 25th, 2006. In total, 30 NLIW events were counted and reconstructed as the environment input for the 3D Parabolic Equation (PE) model.
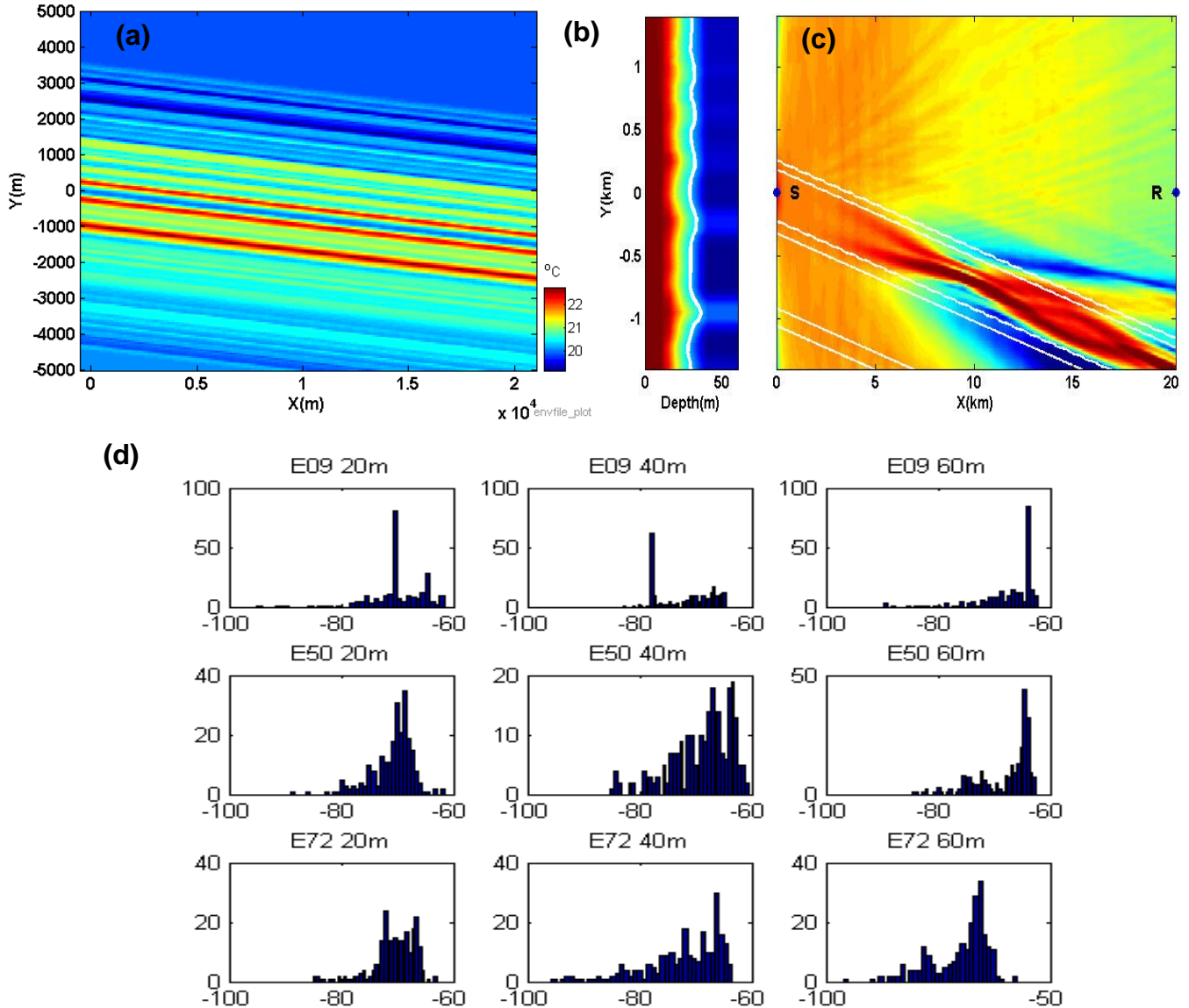

Figure 4 (a) Reconstructed temperature field at 20m water depth using wave parameters extracted from event #72 in SW06 experiment. (b) and (c) Simulated 3D PE modeling result with reconstructed environment shown in Fig. 4(a) as input. (b) shows the water temperature of the vertical cross-section at the source, and (c) shows the depth-integrated acoustic intensity on the horizontal plane. (d) Histogram of acoustic intensity at different depths and IW events.

9

We also improved on the existing 3D PE model with GPU computing technology, resulting in great speed boost. Figure 4 (b) shows the water temperature of the cross-section at the sound source. Figure 4(c) shows the acoustic modeling results using the reconstructed environment as input for the PE model. The isothermal line of 17C degree (shown as the white line) indicates the relative position of the thermalcline in the water column, which clearly shows the incoming internal wave packet. Figure 4(d) shows the histogram of the simulated acoustic intensity at different receiver depth (20, 40 and 60m) and IW event (Event #9, #50 and #72).

B. Mid-to-High Frequency Acoustic Propagation in Shallow Water

We have been studying the propagation and forward scattering of broadband acoustic signals in shallow water regions in the last few years. Several field experiments have been made showing the effects of the water column variability as well as the sea surface of the broadband signal propagation [5,11]. These data indicate that out of plain scattering can be important and there is azimuthal dependency in the acoustic field calculation. To better understand and to predict the acoustic field in these regions requires accurate oceanographic and acoustic models. Recently, we have utilized 2D and 3D PE acoustic propagation models in conjunction with a 3D time-evolving sea surface boundary to analyze the results obtained during a highly calibrated field experiment called KAM11 [5,11]. In this section we present results from our recent modeling efforts.

5. Influence of short time scale water column fluctuations on broadband signal intensity

The KAM11 experiment was conducted during the summer of 2011 in a 100 m shallow water region, near Kauai Island, Hawaii. Two seafloor tripod transceiver systems configured with an 8-element hydrophone arrays and top mounted transducer were deployed 1 km apart. On July 6th from 02:00 to July 7th 02:00 Z, high frequency (25 kHz) chirp signals with a 6 kHz bandwidth were transmitted 138 times over a 20 s sequence between these arrays. Variable wind speeds with consistent direction during the acoustic transmissions was measured showing multiple shifts in direction with maximum and minimum values shown in Fig. 5(c). Surface wave height and direction were measured by a wave rider buoy. Surface wave spectrum and wave height are shown as a function of geotime Figs. 5(a) and 5(b) respectively. These measurements were used to construct the 3D surface wave variations for input to the PE model. The water column was also measured by a thermistor chain deploy near the array configuration. Variations of the thermocline over geotime indicate sharply delineations at T1 to increasing "tiered" temperature profile at geotimes T2, T3 and T4 shown by vertical black lines in Fig. 5. Impulse response measurements in Fig. 5(e) show intermediate arrivals between direct-path/bottom-bounce and surface-bounce signals. Focusing and defocusing of the intermediate direct-path arrivals around 5 ms in Fig. 5(e) show the influence of fluctuations in the sound speed profile over time scales from seconds to hours. Short term intensity variations arise from the vertical variations in the water column. Over longer time scales, changes in the thermocline and the surface conditions govern the evolution of the surface bounce arrival. Data model comparison is conducted with ray tracing and parabolic equation modeling shown next.
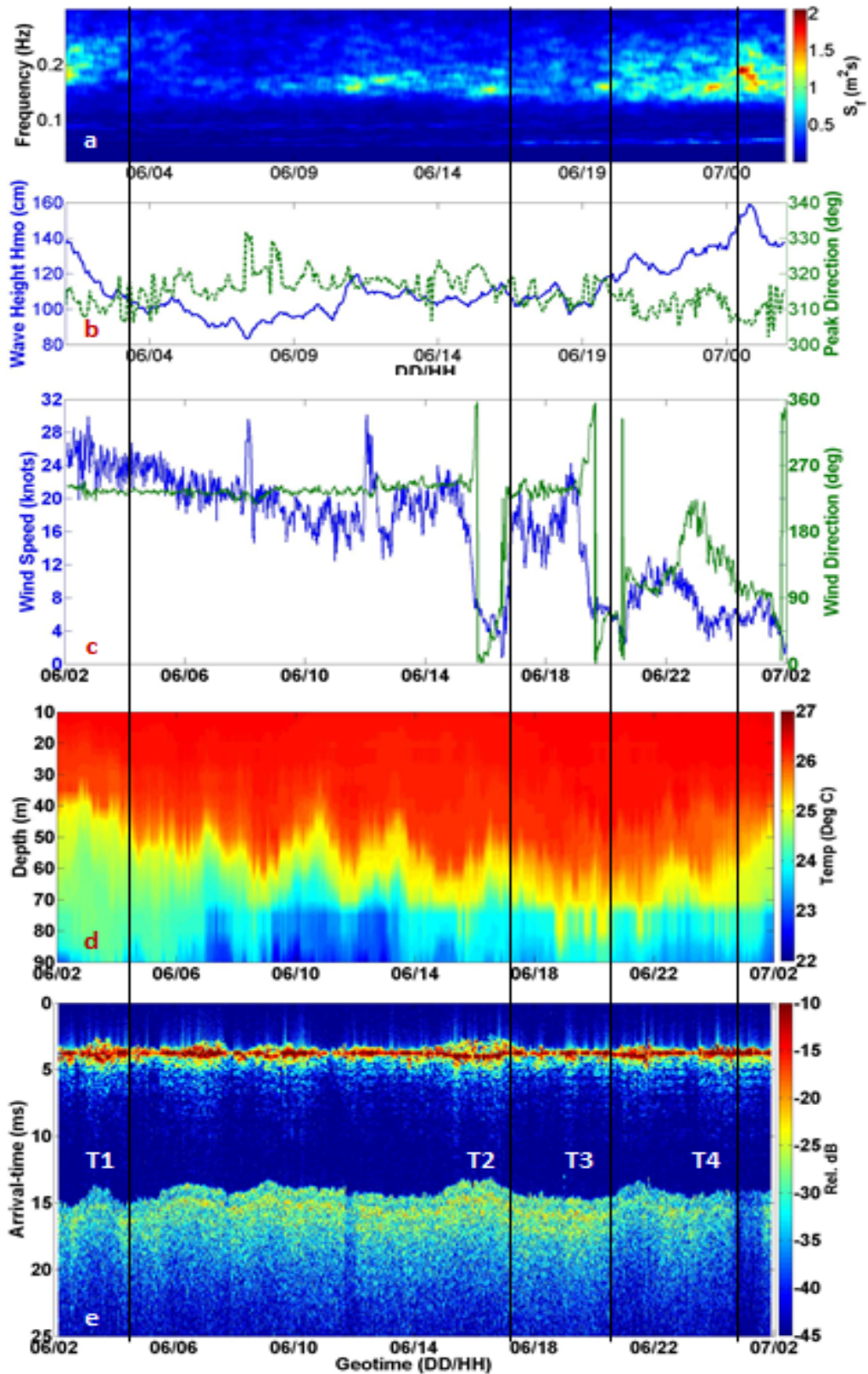
Fig. 5. (a) Waverider buoy surface power spectral density, (b) Wave height and peak direction, (c) Wind speed and direction, (d) Thermistor Diagram, (e) Measured impulse response for duration of deployment with times of interest indicated. Selected times, T1 through T4 are shown by vertical black lines for further analysis.
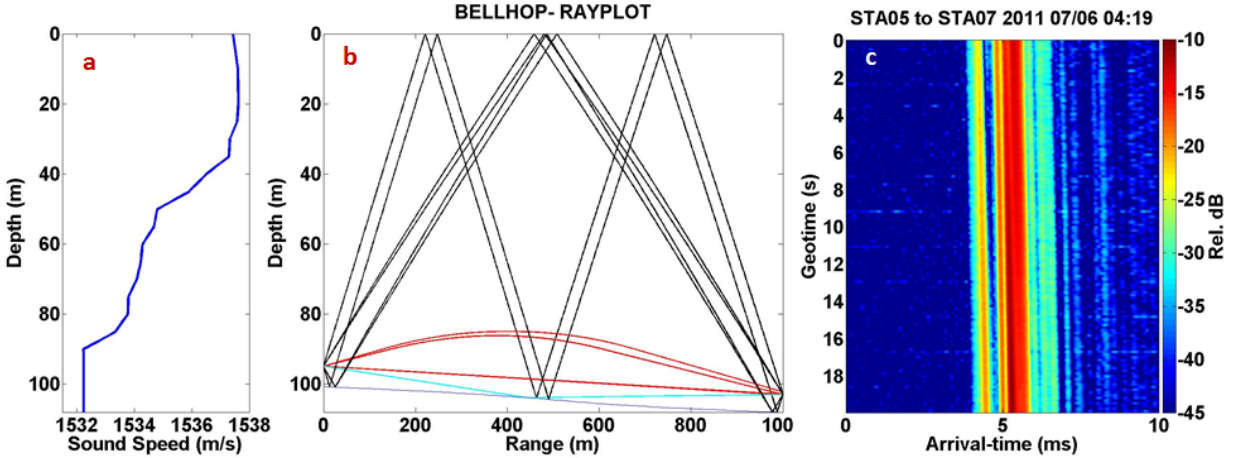
Fig. 6. (a) Sound speed profile for BELLHOP at T1.   (b) BELLHOP output with refracted (bottom trapped) direct path rays.   (c) Measured impulse response at T1 with "banding" in direct path.

Figure 6 shows an example of a sound speed profile (SSP) (Fig. 6(a)) for which ray calculations clearly shows different arrival paths (Fig. 6(b)) corresponding to the measured channel impulse response (Fig. 6(c)). In Fig. 6(a), the SSP is downward refracting at T1 and results in multiple direct path arrivals as modeled by ray theory in Fig. 6(b). This is also seen in the measured impulse response in Fig. 6(c) around arrival time ~ 5 ms. Downward refraction in the water column during this deployment is dependent on minute scale velocity fluctuations in the SSP. As the water column goes through changes, other times shown in Fig. 5(e) are analyzed. At T2, the SSP has a single tier between 40-80 m depth (a) and the intensity range of the surface reflection is -20 to -30 dB. At T3, the SSP has developed a second tier at 60 m depth (d) and surface reflection has been attenuated an additional 5 dB. At T4 the SSP has multiple tiers between 40-90 m depth and the surface reflection has been further weakened to the -35 to -45 dB range.

Figure 7 shows the acoustic measurements for T2, T3, and T4 periods accompanied by 2D PE model with rough surface, the measured acoustic data from the KAM11 experiment shows the influence of short time scale water column fluctuations on high frequency, broadband signal intensity. Simulations with BELLHOP show ray path separation of direct path arrivals under the thermocline. PE simulations are a qualitative fit for the decay of surface bounce signal intensity under an increasingly stratified SSP profile. Arrival time separation in the direct path signals are currently under further examination.
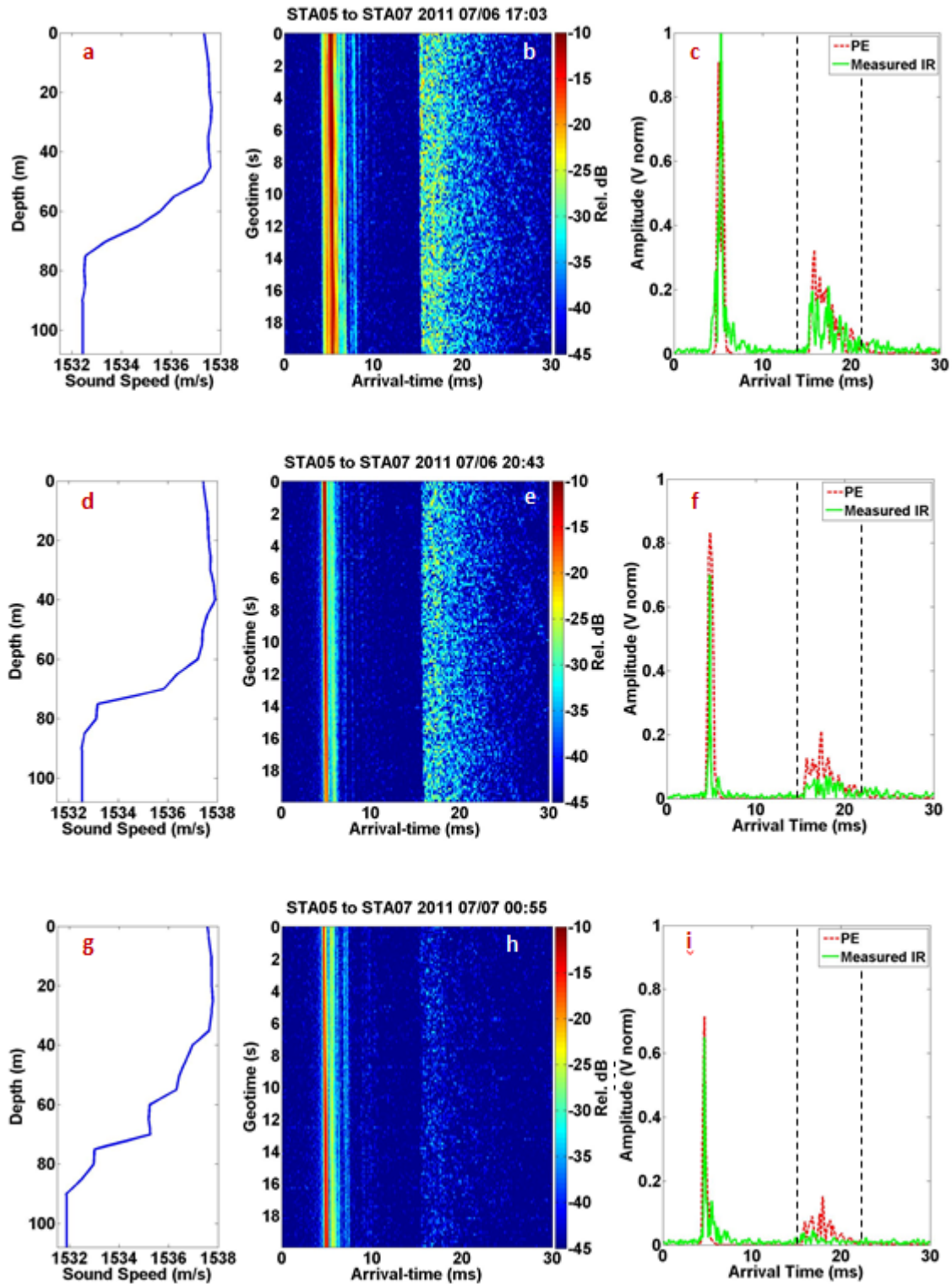
Fig. 7. (a) sound speed profile, (b) measured impulse response, and (c) IR vs. PE amplitude during time T2. (d) sound speed profile, (e) measured impulse response, and (f) IR vs. PE amplitude for time T3. (g) sound speed profile, (h) measured impulse response, and (i) IR vs. PE amplitude for time T4.

C. Development of time-reversal acoustic modem

Digital-signal-processor (DSP) implementations of a low-complexity high-frequency underwater communication system were developed. Both the transmitter and receiver were implemented on a hardware development platform, as shown in Figure 8. Multiple field tests were conducted in shallow water conditions in Lewes, Delaware. The receiver uses time-reversal multichannel combining followed by a single channel decision feedback equalizer to mitigate the inter-symbol interference in the underwater acoustic environment. Periodic channel estimation was employed to deal with the rapid channel fluctuations. Various optimization techniques were utilized to improve the performance and execution time of our receivers. Their effectiveness was demonstrated through simulations and experimental results. Furthermore, a fast implementation of the matching pursue channel estimation method was used. Its performance was compared to that of the basic matching pursuit algorithm. Experimental results showed successful binary phase-shift keying (BPSK) transmissions at three different symbol rates. Low bit error rates were achieved as shown in Figure 9.
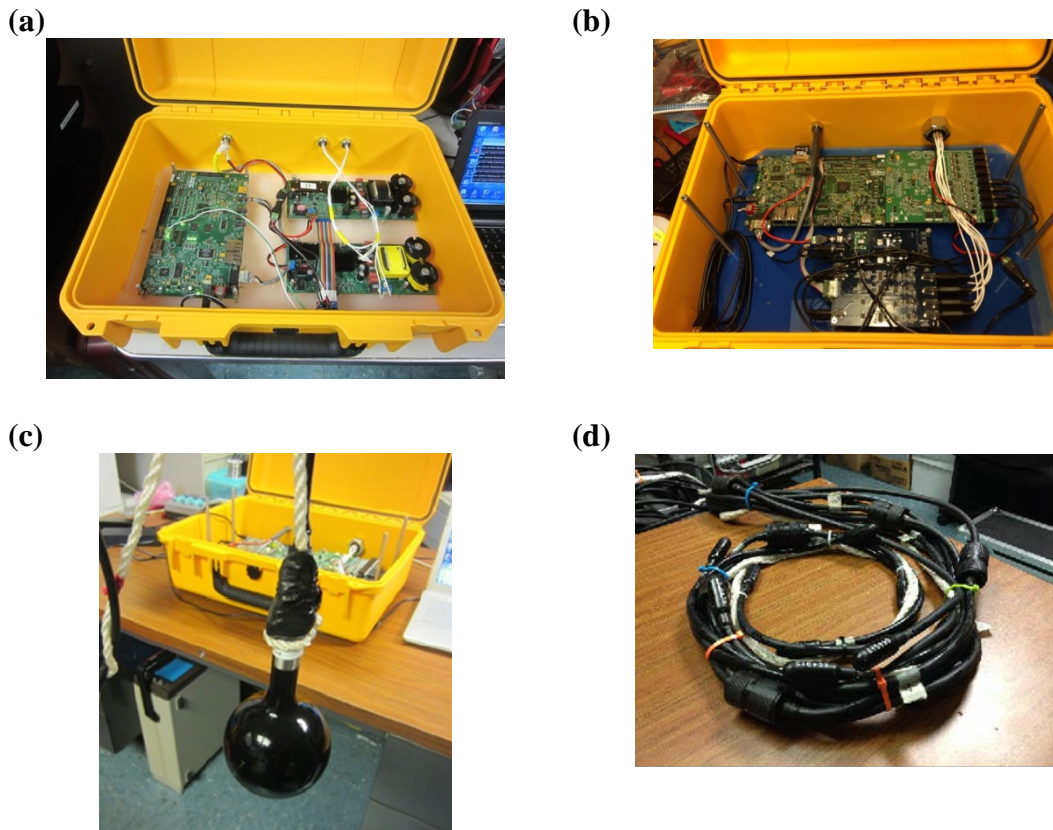
(a)

(b)

(c)

(d)

Figure 8. Acoustic modem hardware purchased from Aquatic Sensor Network Inc. (a) Transmitter box. (b) Receiver box. (c) Transducer. (d) Receiver array.

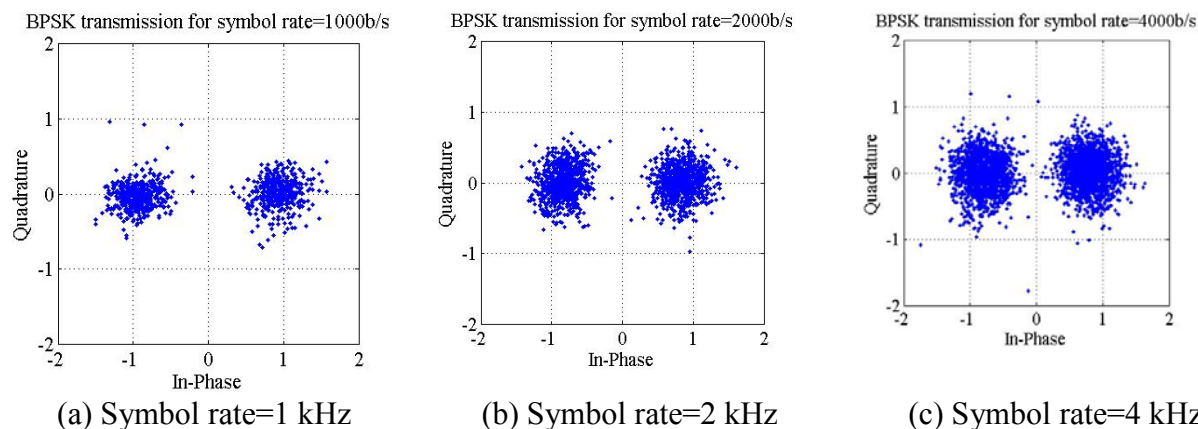(a) Symbol rate=1 kHz   (b) Symbol rate=2 kHz   (c) Symbol rate=4 kHz

Figure 9. Scatter plots from the field trip on September 18, 2014 to the Delaware Bay. At the symbol rate of 1 and 2 kHz, no errors were reported. At the rate of 4 kHz, the bit-error-rate is 0.03%.

IMPACT/APPLICATIONS

The low frequency component of our research contributes to the understanding of acoustic propagation in complex shallow water regions. We have developed a model that is able to reproduce the mechanism of acoustic intensity variation due to internal waves and to quantitatively predicts the time and location of specific details. The high frequency part of our research has contributed to the understanding of the effects of surface wave roughness and directionality as well as bubble effects on sound propagation, which in turn affect the performance of acoustic communication signals.

RELATED PROJECTS

We have been working with Drs. Lynch, Duda, and Lin from Woods Hole Oceanographic Institute (WHOI) and Dr. K. B. Smith from Naval Post Graduate School. Part of our work in instrumentation is also related to our DURIP project (N00014-12-1-0789) [12].

REFERENCES

[1]   J. Luo, M. Badiey, E. A. Karjadi, B. Katsnelson, A. Tskhoidze, J. F. Lynch, and J. N. Moum, "Observation of sound focusing and defocusing due to propagating nonlinear internal waves," *J. Acoust. Soc. Am.*, 124(3), EL66–EL72, (2008).

[2]   W. S. Hodgkiss, *et al.*, "Kauai Acomms MURI 2008 (KAM08) Experiment Trip Report,".

[3]   W. S. Hodgkiss, *et al.*, (2011)"Kauai Acomms MURI 2011 (KAM11) Experiment Trip Report,".

[4]   M. Badiey, L. Wan, and A. Song, "Three-dimensional mapping of evolving internal waves during the Shallow Water 2006 experiment," J. Acoust. Soc. Am., 134(1), EL7-EL13, (2013).

[5]   J. Eickmeier, and M. Badiey, "Influence of short time scale water column fluctuations on broadband signal intensity," J. Acoust. Soc. Am. 135, 2305 (2014).

[6]   M. Badiey, L. Wan, and Lynch, J., "Statistics of internal wave during the SW06 experiment," J. Acoust. Soc. Am., 134(5), 4035, (2013).

[7]   L. Wan, M. Badiey, and Lynch, J., "Acoustic normal mode fluctuations due to internal waves in the Shallow Water 2006 experiment," J. Acoust. Soc. Am., 134(5), 4036 (2013).

[8]   W. A. Kuperman, W. S. Hodgkiss, H. C. Song, T. Akal, C. Ferla, and D. R. Jackson, "Phase conjugation in the ocean: Experimental demonstration of an acoustic time-reversal mirror," J. Acoust. Soc. Am. 103(1), 25-40 (1998).

[9] D. Rouseff, D. R. Jackson, W. L. J. Fox, C. D. Jones, J. A. Ritcey, and D. R. Dowling, "Underwater acoustic communication by passive-phase conjugation: Theory and experimental results," IEEE J. Oceanic Eng. 26(4), 821-831 (2001).

[10] L. Wan, J. X. Zhou, and P. H. Rogers, "Low-frequency sound speed and attenuation in sandy seabottom from long-range broadband acoustic measurements," J. Acoust. Soc. Am., 128(2), 578-589 (2010).

[11] M. Badiey, J. Eickmeier, and A. J. Song, (2014) "Arrival-time fluctuations of coherent reflections from surface gravity water waves", J. Acoust. Soc. Am., 135(5), EL226-231.

[12] ONR DURIP: Development of high data rate acoustic multiple-input/multiple-output modems, Grant N00014-12-1-0789.

PUBLICATIONS

[1] Badiey, M., Wan, L., and Lynch J. F., (2013) "Statistics of internal waves measured during the Shallow Water 2006 experiment", J. Acoust. Soc. Am., 134(5), 4035.

[2] Badiey, M., and Luo. J., (2013) "Time reversal of modal arrivals for broadband signals in horizontally stratified shallow water due to internal waves", J. Acoust. Soc. Am., 134(5), 4036.

[3] Song, A. J., and Badiey, M., (2013) "Time reversal methods for high frequency multiple-input/multiple-output underwater acoustic communication", J. Acoust. Soc. Am., 134(5), 4033.

[4] Wan, L., Badiey, M., and Lynch J. F., (2013) "Acoustic normal mode fluctuations due to internal waves in the Shallow Water 2006 experiment", J. Acoust. Soc. Am., 134(5), 4036.

[5] Wan, L. and Badiey, M., (2014) "Coherence measurements of acoustic normal modes during one month of internal wave events on the New Jersey continental shelf"J. Acoust.Soc.Am.,135(4).

[6] Badiey, M., Eickmeier, J. and Song, A. J., (2014) "Arrival-time fluctuations of coherent reflections from surface gravity water waves", J. Acoust. Soc. Am., 135(5), EL226-231.

[7] Eickmeier, J. and Badiey, M., (2014) "Influence of short time scale water column fluctuations on broadband signal intensity", J. Acoust. Soc. Am., 135(4), 2305.

[8] Badiey, M., and Song, A. J., (2014) "Low frequency acoustic communication and the waveguide modal behavior during Shallow Water 2006 experiment", J. Acoust. Soc. Am., 135(4), 2431.

[9] Badiey, M., Wan, L., and Lynch J. F., (2014), "Statistics of nonlinear internal waves during the Shallow Water 2006 experiment", submitted to J. Acoust. Soc. Am. Express Letter.

[10] H. Yu, A. Song, M. Badiey, F.-J. Chen, and F. Ji, (2013) "Iterative Estimation of the Time-Varying Underwater Acoustic Channel Using Basis Expansion Models", 8th ACM International Conference on Underwater Networks & Systems (WUWNet'12), Kaohsiung, Taiwan.

[11] S. Matiz, A. Song, M. Badiey, "DSP Implementation of Time-Reversal Receivers", (In Preparation), Marine Technology Society Journal, 2014.